POLITECNICO DI TORINO
Repository ISTITUZIONALE

Experimental evidences of flexural to shear to crushing failure mode transition in reinforced concrete beams without stirrups

Original
Experimental evidences of flexural to shear to crushing failure mode transition in reinforced concrete beams without stirrups / Corrado, M., Ventura, G., Carpinteri, A.. - In: ENGINEERING STRUCTURES. - ISSN 0141-0296. - STAMPA. - 271:(2022), p. 114848. [10.1016/j.engstruct.2022.114848]

Availability:
This version is available at: 11583/2972567 since: 2022-10-24T20:52:12Z

Publisher:
Elsevier

Published
DOI:10.1016/j.engstruct.2022.114848

Terms of use:

This article is made available under terms and conditions as specified in the corresponding bibliographic description in the repository

Publisher copyright
Elsevier postprint/Author's Accepted Manuscript

© 2022. This manuscript version is made available under the CC-BY-NC-ND 4.0 license
http://creativecommons.org/licenses/by-nc-nd/4.0/.The final authenticated version is available online at:
http://dx.doi.org/10.1016/j.engstruct.2022.114848

(Article begins on next page)

20 November 2026

Experimental evidences of flexural to shear to crushing failure mode transition in reinforced concrete beams without stirrups

M. Corrado[a,*], G. Ventura[a], A. Carpinteri[a]

[a] *Department of Structural, Geotechnical and Building Engineering, Politecnico di Torino, Corso Duca degli Abruzzi 24, 10129 Torino, Italy*

Abstract

The results of a series of experimental bending tests carried out on reinforced concrete members without transverse reinforcement are reported and illustrated as a contribution to the study of the flexural to shear to crushing failure mode transition. A total of 45 beams were tested to investigate the effects of a wide range of longitudinal reinforcement amounts –0.25% to 3.39%–, beam depths –5 to 80 cm– and beam slendernesses –3 to 24–. The analysis of the experimental data encompasses the identification of the overall mechanical response, the assessment of the ultimate load and the detection of the critical crack that leads to the final collapse of the beam. The results are interpreted with reference to a global failure mode transition scheme, which allows to analyse all the failure modes within the same framework. As a result, an effective and synthetic prediction of the failure mode transition is achieved on the basis of dimensionless numbers, namely N_P, N_C and λ_l, defined in the framework of linear elastic fracture mechanics. Besides, strengths and weaknesses of the provisions of some codes of practice are highlighted on the basis of the experimental results. In this context, some drawbacks are reported for what concerns the inclusion of the size effect in the models provided to assess the shear capacity of reinforced concrete beams.

Keywords: reinforced concrete, shear strength, failure mode transition, size effect, critical crack

2010 MSC: 00-01, 99-00

*Corresponding author
Email address: mauro.corrado@polito.it (M. Corrado)

1. Introduction

The determination of the shear strength of reinforced concrete (RC) beam elements without transverse reinforcement has been deeply investigated in literature since the beginnings of the development of RC technology. One of the earliest studies is due to Slater et al. [1], published in 1926. Since then, many efforts have been done by the international scientific community to reach a comprehensive understanding and modelling of the shear resistance mechanism, which depends on a complex interaction among material properties, amount of longitudinal reinforcement, effective depth, local stress transfer mechanisms (aggregate interlock and dowel action), etc. Research has been conducted on many fronts: an intense experimental activity that is being carried out worldwide for more than 70 years [2, 3, 4, 5, 6, 7] bringing to the creation of a huge database (for instance, the results of more than 1800 tests were collected by Collins and co-workers on 2008 [8]), has been accompanied by empirical analysis [9, 10, 11, 12, 13], theoretical studies [14, 15, 16, 17] and numerical approaches [18, 19, 20].

One of the most delicate aspects, which is still under debate and, therefore, is not satisfactorily addressed in the Standards [21, 22, 23, 24], is the effect of the structural size. Particularly interesting contributions were provided by Bažant and co-workers [4, 25, 26, 27, 28, 29, 30, 31] who discussed the results of experimental tests, compared several size effect formulas and evidenced the limitations of experimental data, by Vecchio, Collins and co-workers [32, 33, 8] who developed the *Modified Compression Field Theory*, and by Muttoni and co-workers [34, 35, 16] who proposed the *Critical Shear Crack Theory*. Another remarkable line of studies is due to Carpinteri and co-workers who proposed an approach to the problem based on fracture mechanics and dimensional analysis background and performed several experimental tests. They initially studied the problem of minimum reinforcement in RC beams and the related brittle or ductile bending failure mechanism [36, 37, 38, 39, 40, 41, 42, 43]. These studies were then extended to include the effect of fibres reinforcement [44, 45, 46], shear and concrete crushing failures [47, 17, 48, 49], influence of axial force [50] and the size effects, which are introduced through dimensionless brittleness numbers. Structural elements with the same brittleness number will show the same mechanical behaviour. The works by Carpinteri and co-authors share the common idea that failure is caused by the formation and propaga-

tion of a critical crack. This concept has been used both for the early works on bending failure and specifically in mixed bending/shear works where the shape of the critical crack was reported from experimental testing [17, 48]. The concept of critical crack has been also extensively used by Muttoni et al. [34, 35, 16, 51, 52], being the prediction of the shear strength obtained by the *Critical Shear Crack Theory* based on the shape of the critical crack, its width and its roughness.

The present paper reports and illustrates the results of a series of experimental tests aimed at finding an experimental confirmation of the *global failure mode transition scheme* theoretically introduced by Carpinteri et al. [53, 54] and shown in Fig. 1. According to this scheme, a double transition from flexural to shear failure and from shear to crushing failure is obtained: (1) by increasing the reinforcement area, path (d)-(e)-(f); (2) by decreasing the scale with constant reinforcement area, path (a)-(e)-(i); (3) by increasing the scale with constant reinforcement percentage, path (g)-(e)-(c); and (4) by decreasing the beam slenderness, path (h)-(e)-(b). In the context of the present work, the three failure modes are defined as follows:

- the *flexural failure mode* is characterized by the propagation of a main flexural crack close to the mid-span cross section, propagating almost straightly from the tensile to the compression chord of the beam. The final collapse is due to the yielding and tensile rupture of the reinforcing bars, which is typical of RC beams with a low amount of reinforcement.

- the *shear failure mode* is obtained when a shear crack propagates from the bottom to the top side of the beam, leading to a separation of the beam in two blocks connected only by the longitudinal reinforcement, which remains in the elastic regime. The shape of the critical crack is such that no further load-carrying mechanisms are possible. Consequently, the global response is characterised by a vertical drop in the load-carrying capacity after the peak load.

- the *crushing failure mode* is almost similar to the shear mode except for the fact that, once the shear crack reaches the top chord of the beam, a residual load-carrying mechanism is activated, which consists in an arch or a strut action that takes the load directly to the supports. Both mechanisms involve an increase of

the compression stress in the region above the shear crack, until a buckling failure is achieved (the compressed strut is quite slender), made evident by the expulsion of a wedge-shaped portion of beam near the load application point. It has to be remarked that with the beam geometry and load setup considered in the present work, the ultimate compression strain of concrete is difficult to reach because of an insufficient confinement. In the crushing failure mode, the peak load, which is attained when the shear crack is completely propagated, is typically followed by a partial recovery of the load-carrying capacity due to the arch or strut action.

The three failure mechanisms have very different crack patterns and overall mechanical responses: from brittle flexural collapse, typical of under-reinforced RC beams, to ductile behavior with the formation of plastic hinges, typical of lightly-reinforced RC beams, to brittle failure ruled by concrete crushing, typical of over-reinforced RC elements.

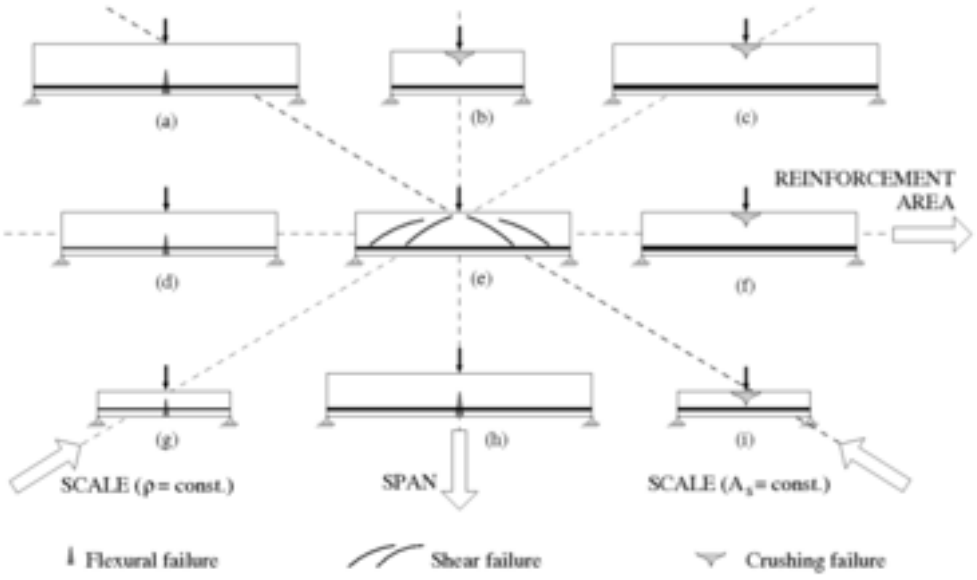


Figure 1: Global failure mode transition scheme.

Besides confirming the global failure mode transition scheme by means of experimental results, the aim of this work is to provide the scientific community with the data of a series of experiments for the study of the size effect in RC beams without transverse reinforcement. Compared to other experimental tests reported in literature, the peculiar

value of this study is given by the fact that different parameters were individually varied (cross section, reinforcement percentage, reinforcement area, span) keeping constant all the others. In total 45 beams were tested. The outline of the paper is as follows: Section 2 is devoted to the description of the experimental program, whose results are described in Section 3, by detailing the effects of the reinforcement amount and the beam size and slenderness. In Section 4 the experimental results are compared to the predictions of some codes of practice so as to evidence strengths and weaknesses of the models currently used by practitioners to determine the shear capacity of RC beams. Section 5 presents a discussion of the experimental results in terms of load carrying capacity and shape of the critical crack. Finally, conclusions are drawn in Section 6.

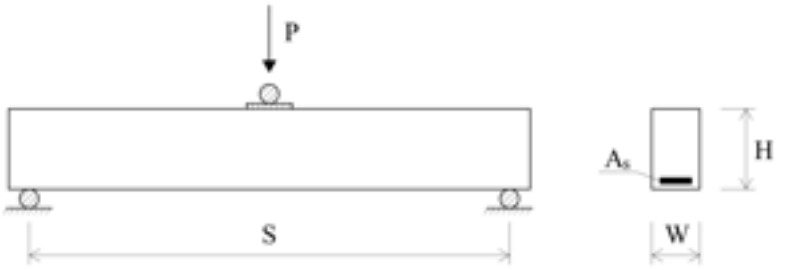
2. Experimental program

An extended experimental program was carried out at the Laboratory of Materials and Structures of Politecnico di Torino (Italy) to study the failure mechanism and the crack pattern in concrete beams reinforced only with longitudinal bars. The testing program was designed on the basis of the global scheme illustrating the failure mode transitions shown in Fig. 1.

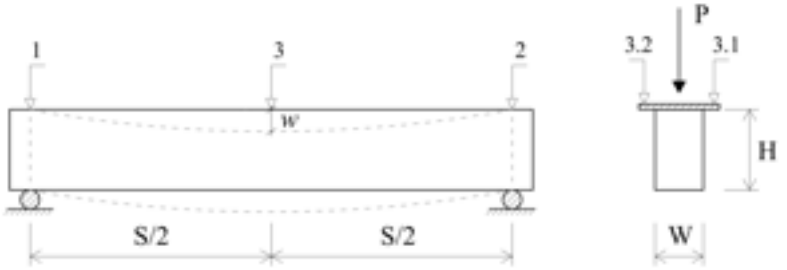
2.1. Specimen geometry and test setup

The tested specimens had span S and rectangular cross section of depth H and width W variable depending on the considered case. Longitudinal reinforcement of area A_s was provided on the bottom side of each beam, whereas transverse reinforcement against shear failure was not provided. The longitudinal bars were arranged in one to three layers, depending on the reinforcement amount. The beams were simply supported and loaded in three-point bending (see Fig. 2).

Four series of specimens were tested, for a total of 15 different types of beam, in order to analyze all the four transitions depicted in Fig. 1. The geometrical parameters and the amount of longitudinal reinforcement of all the beams are reported in Tab. 1, where the bold numbers evidence the investigated parameter. The shear slenderness, λ_l, is the shear span to beam depth ratio, $S/(2H)$, and ρ is the percentage of longitudinal reinforcement, equal to $100A_s/(WH)$. It is worth noticing that the normalization of



(a)



(b)

Figure 2: Test setup: (a) load configuration; (b) position of the measuring devices.

all the parameters is done with respect to the overall depth, H, instead of the effective depth, d, that is typically used by the Standards, to be coherent with the definition of the dimensionless parameters N_{P} and N_{C} [37, 17, 55] that will be used in the next Sections for the interpretation of the results.

Each beam type is identified by a label having the following structure: Hxx_$\rho y.yy$_Szzz, where xx stands for the beam depth in cm, $y.yy$ is the percentage of longitudinal reinforcement and zzz stands for the beam span in cm.

The first series of specimens listed in Tab. 1 was designed to investigate the effect of the reinforcement amount (path (d)-(e)-(f) in Fig. 1); the second and third ones the effect of the beam size for a constant reinforcement ratio and area, respectively (paths (a)-(e)-(i) and (g)-(e)-(c) in Fig. 1); and the fourth one the effect of the slenderness (path (b)-(e)-(h) in Fig. 1). For each beam type, three specimens were prepared and tested, in order to have some statistics of the results.

All the tests were carried out in deflection-control, having assumed the mid-span

Table 1: Series of specimens

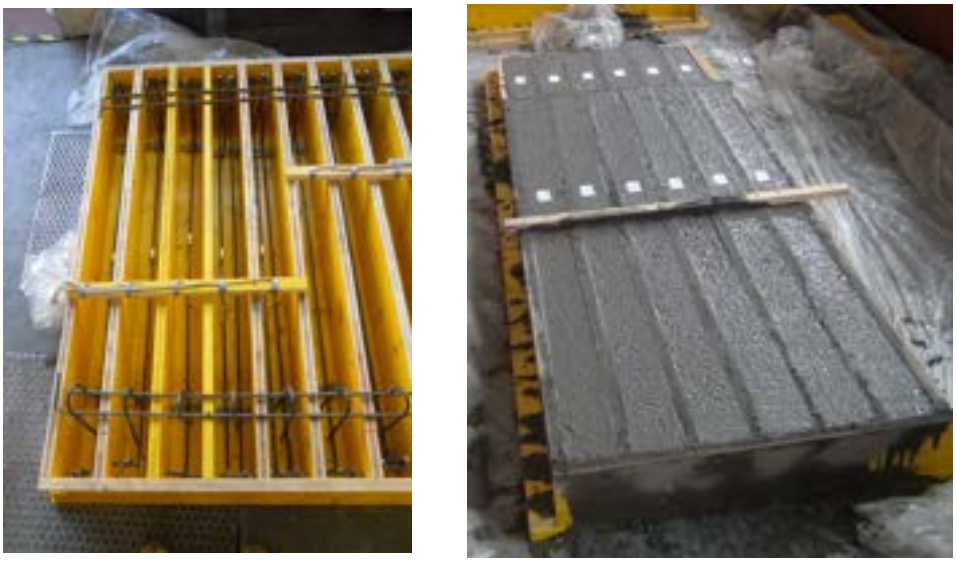
	Id. code	W (mm)	H (mm)	S (mm)	λ_l	A_s	ρ (%)
Effect of steel reinforcement ratio	H20_ρ0.25_S120	100	200	1200	3	1ϕ8	**0.25**
	H20_ρ0.50_S120	100	200	1200	3	2ϕ8	**0.50**
	H20_ρ1.13_S120	100	200	1200	3	2ϕ12	**1.13**
	H20_ρ2.26_S120	100	200	1200	3	4ϕ12	**2.26**
	H20_ρ3.39_S120	100	200	1200	3	6ϕ12	**3.39**
Size effect with constant reinf. ratio	H05_ρ1.01_S030	100	**50**	300	3	1ϕ8	1.00
	H10_ρ1.13_S060	100	**100**	600	3	1ϕ12	1.13
	H20_ρ1.13_S120	100	**200**	1200	3	2ϕ12	1.13
	H40_ρ1.13_S240	200	**400**	2400	3	8ϕ12	1.13
	H80_ρ1.13_S480	300	**800**	4800	3	24ϕ12	1.13
Size effect with constant reinforcement area	H10_ρ2.26_S060	100	**100**	600	3	2ϕ12	2.26
	H20_ρ1.13_S120	100	**200**	1200	3	2ϕ12	1.13
	H40_ρ0.28_S240	200	**400**	2400	3	2ϕ12	0.28
	H80_ρ0.09_S480	300	**800**	4800	3	2ϕ12	0.09
Effect of beam slenderness	H20_ρ1.13_S060	100	200	600	**1.5**	2ϕ12	1.13
	H20_ρ1.13_S120	100	200	1200	**3**	2ϕ12	1.13
	H20_ρ1.13_S240	200	200	2400	**6**	2ϕ12	1.13
	H20_ρ1.13_S480	300	200	4800	**12**	2ϕ12	1.13

deflection as the control parameter, up to the complete collapse of the beam. To this purpose, two LVDTs were placed at the mid-span cross section, one per each side of the beam, and their values averaged to compute the deflection, δ, afterwards used to plot the load-deflection curves. Besides, two LVDTs were installed at the beam ends, on the upper side, in order to measure possible settlements at the supports (see Fig. 2). Such a setup and testing control allowed to capture the post-peak ductile or softening behavior typical of flexural failure, whereas it was not sufficient to control the brittle

events leading to abrupt drops in the load carrying capacity that usually characterize shear and crushing failures. The concentrated load, P, was applied at the mid-span by means of hydraulic jacks with the interposition of a loading plate having a width equal to 5% of the beam span. The evolution of the crack pattern was not monitored continuously during the tests, but the final crack pattern on both sides of the specimen was acquired by means of a high resolution digital camera after the end of each test. In order to have the picture of the complete crack pattern, all the cracks that were developing along the beam were marked step-by-step with a black felt-tip pen. They were also numbered to record the correct sequence of formation and propagation of the cracks. The recorded images have been processed to extract the critical crack. The width of the critical crack was not measured during the tests.

2.2. Material properties and specimen preparation

A single batch of concrete was prepared in a mixing plant and delivered to the Laboratory of Materials and Structures of Politecnico di Torino, where it was cast in formworks where the reinforcements were previously arranged (see Fig. 3). The main prescriptions for concrete were: strength class, as defined by EN 1992-1-1 [24], equal to C35/45, maximum aggregate size equal to 20 mm, consistence class S5 (defined through the slump test according to EN 12350-2 [56]), and exposure class XC1. The actual mechanical properties of concrete were assessed with specific tests carried out at the 28th day after casting. The compressive strength, $f_{c,cube}$, was measured on 150 x 150 x 150 mm cubic specimens, following the Standards EN 206-1 [57] and EN12390-3 [58], the secant value of the elastic modulus, E_c, was assessed on cylindrical specimens 100 mm in diameter and 300 mm in depth, according to the Italian Standard UNI 6556:1976 [59], the fracture energy, G_F, was evaluated by means of three-point-bending tests carried out on pre-notched beams following the procedure prescribed by RILEM recommendation TC-89 [60]. Six specimens have been tested for each property. The mean values and the standard deviations of the mechanical properties are reported in Tab. 2. The cylindrical strength has been computed by the formula $f_c = 0.85 f_{c,cube}$. All the beams were tested within a month from the 28th day of concrete curing in order to limit the variability of the mechanical properties between the first and the last tested beam and to use, with acceptable accuracy, the properties evaluated at the 28th day for the analysis of the results and the



(a) (b)

Figure 3: Specimen preparation: (a) formworks; (b) concrete casting.

application of the formulae provided by the Standards.

As regards the reinforcement bars, only two diameters have been used, 8 and 12 mm, in order to limit the effect of the steel-concrete bond properties (note that 8 mm bars were used to provide the correct amount of reinforcement only in the case of very low percentages). The commercial B450C steel was used, characterized by a nominal yielding strength of 450 MPa and an ultimate strength of 540 MPa. The actual material properties of the reinforcing bars were determined by means of uniaxial tensile tests carried out on four samples for each diameter, following the prescriptions of the Standards EN ISO 15630-1 [61] and ISO 6892-1 [62]. The mean yielding, f_y, and ultimate, f_t, strengths obtained for the two diameters are reported in Tab. 3.

Table 2: Mechanical properties of concrete

$f_{c,cube}$ (MPa)	Standard deviation	f_c (MPa)	E_c (MPa)	Standard deviation	G_F (N/m)	Standard deviation
47.9	4.6	39.8	29595	289	172.9	14.7

Table 3: Mechanical properties of steel

ϕ (mm)	f_y (MPa)	Standard deviation	f_t (MPa)	Standard deviation
8	502	11.6	611	9.1
12	513	3.2	603	1.6

3. Experimental results

In the present section, the results of the experimental tests are presented and discussed. Even though very different crack patterns were obtained by varying the reinforcement ratio and geometrical parameters, they presented some common features. Attention is devoted to the determination of position and shape of the crack whose opening finally determines the beam failure, which is referred to as *critical crack* in the following.

3.1. Effect of the reinforcement amount

The first series of specimens was designed to analyze the effect of the reinforcement amount on the load-carrying capacity and the crack pattern, experimentally evidencing flexural to shear to crushing failure transitions in RC beams. It consists of 5 types of beams, having the same size and different reinforcement percentages, ρ, varying in the range 0.25% to 3.39% (see Fig. 4). This set of specimens allows to follow the transition along the path (d)-(e)-(f) shown in Fig. 1.

In the case of ρ equal to 0.25%, beams labeled H20_ρ0.25_S120, the load-deflection behavior was linear elastic up to the cracking load, which was about 15 kN, when a flexural crack appeared very close to the mid-span cross section of the beam. Such a circumstance provoked a sudden decrease of the load-carrying capacity and stiffness, with the reinforcing bar still in the elastic regime. Afterwards, the load increased again, up to the yielding and hardening of the reinforcement. During the hardening phase two more cracks appeared, symmetrically placed at about $S/8$ from the beam midspan. The final collapse of the beam was due to the rupture of the reinforcing bars. The overall behavior was very ductile, with the ultimate deflection equal to $0.015S$. The load-deflection curves and the trajectory of the critical crack of the three beams H20_ρ0.25_S120 are shown in

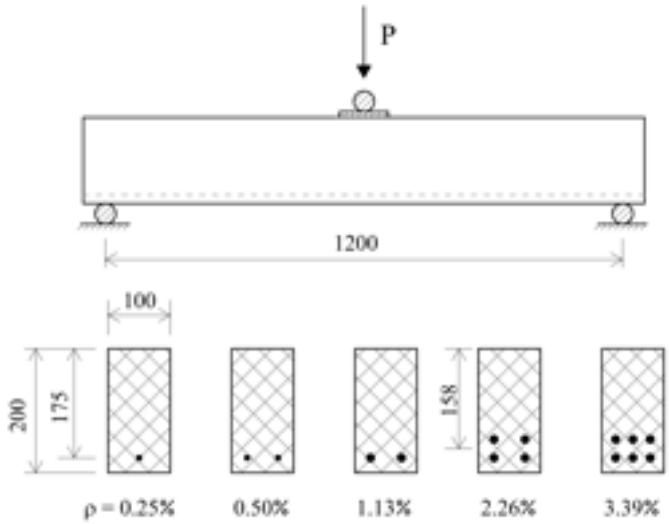


Figure 4: Set of beams used to analyze the effect of the reinforcement amount, ρ.

Fig. 5a. The trajectory of the cracks are reported in dimensionless form, with the abscissa normalized with respect to the shear span, S, and the ordinate with respect to the beam depth, H. Two trajectories are shown for each beam, one referred to the front side and the other to the back side. A picture of one of the three beams taken after the test is shown in Fig. 6. This is a typical flexural failure.

The load-deflection curves of the beams with $\rho = 0.50\%$, labeled H20_ρ0.50_S120, are characterized by a first steep branch corresponding to the pre-cracking phase, followed by a second branch of reduced stiffness due to the appearance of a first flexural crack close to the mid-span cross section, and a third branch, almost horizontal, consequent to the reinforcement yielding (see Fig. 5b). During the second and the third phases, a number of flexural cracks appeared along the span of the beam, almost equally spaced, from the center toward the supports (cracks numbered as 2, 3 and 4 in Fig. 7). Most of them propagated in the vertical direction only up to $H/2$, except for the two symmetric cracks no. 2, which propagated up to the upper side of the beam, curving toward the load application point. In the ductile phase, i.e. after the reinforcement yielding, the two cracks no. 2 opened more and more, and competed with the central crack. In one case out of three, the collapse of the beam was determined by the rupture of the reinforcement

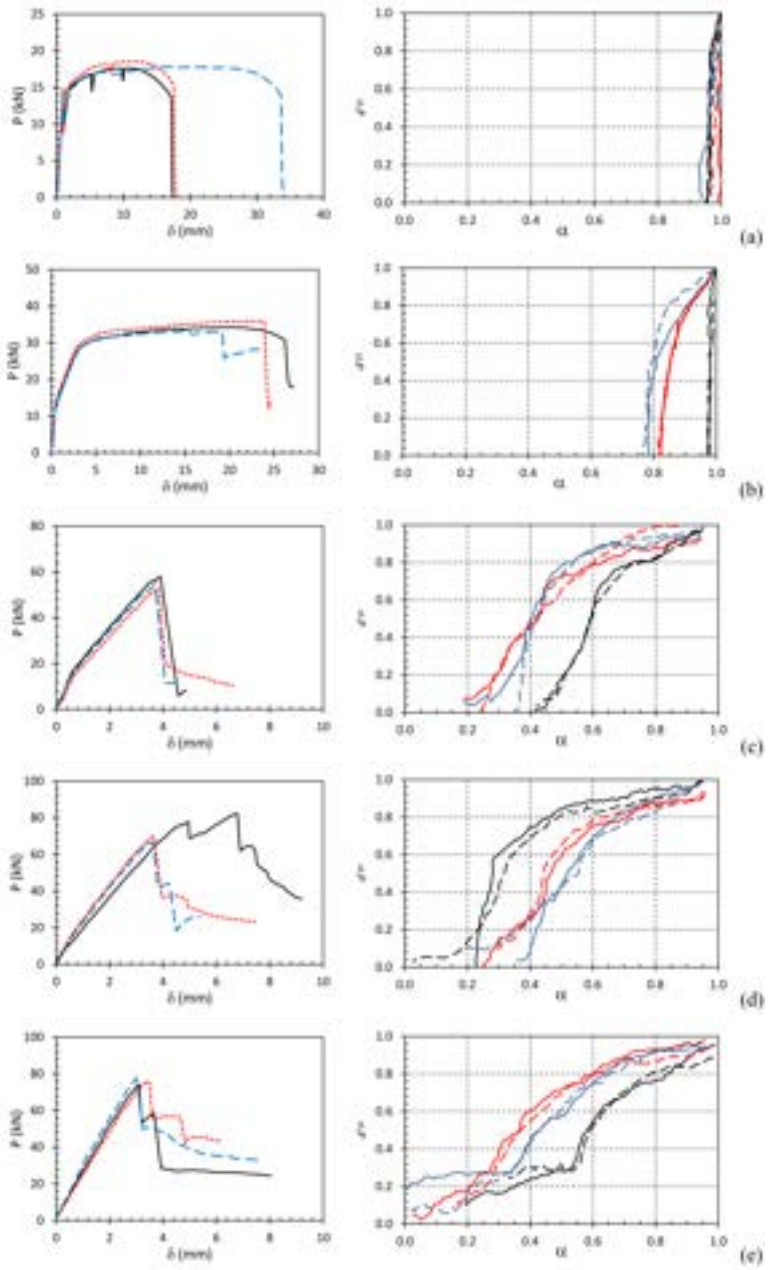


Figure 5: Load vs. mid-span deflection curves and critical crack trajectories for the series of beams designed to analyze the effect of the reinforcement amount: (a) H20_ρ0.25_S120; (b) H20_ρ0.50_S120; (c) H20_ρ1.13_S120; (d) H20_ρ2.26_S120; (e) H20_ρ3.39_S120.

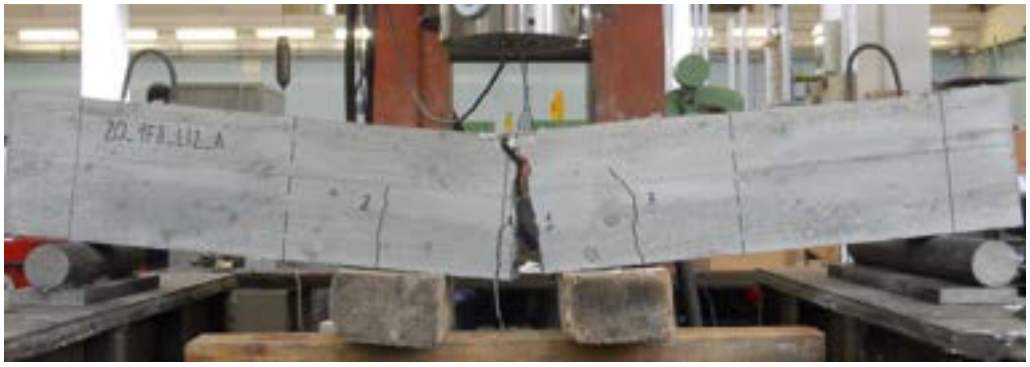


Figure 6: Picture of the beam H20_ρ0.25_S120-A after the test.

within the central crack (pure flexural mode, see Fig. 7a), whereas in the other two cases the collapse was determined by an excessive opening of one of the two symmetric cracks, and the consequent decrease in the aggregate interlocking effect (flexural/shear mode, see Fig. 7b). In all the three cases the overall behavior was very ductile, with an ultimate deflection $\delta = 0.02S$. The critical crack paths for the three beams H20_ρ0.50_S120 are shown in Fig. 5b.

By increasing the reinforcement amount to $\rho = 1.13\%$, beams labeled H20_ρ1.13_S120, the overall behavior became more brittle. The load-deflection curves shown in Fig. 5c consist of three branches: a linear elastic branch up to the cracking load, a second linear branch having reduced stiffness, and a final abrupt drop in the load carrying capacity. Most of the crack pattern developed during the second phase. First, a series of flexural cracks appeared from the center of the beam span toward the supports. They were approximately spaced by $H/2$. Then, increasing the midspan deflection, another set of flexural cracks appeared, at an intermediate position with respect to the first series of cracks. Finally, by approaching the ultimate load, one of the flexural cracks, positioned at $S/4$ from the mid-span, propagated above the geometrical barycenter of the beam, deflecting toward the load application point driven by the shear stresses (see Fig. 8). Very suddenly, such a crack opened and propagated up to the upper side of the beam, while, on the bottom side, a sub-horizontal crack stemmed due to the dowel action of the reinforcing bars. This crack evolution led to a very brittle failure, without any possibility of recovering partially the load-carrying capacity. The repeatability of this case is very



(a)



(b)

Figure 7: Pictures of the beams (a) H20_ρ0.50_S120-A and (b) H20_ρ0.50_S120-C after the test.

good, the three load-deflection curves shown in Fig. 5c being almost overlapped. The trajectories of the critical cracks of the three beams H20_ρ1.13_S120 are shown in Fig. 5c.

Beams with a reinforcement amount equal to 2.26%, specimens labeled H20_ρ2.26_S120, exhibited a development of the crack pattern similar to the previous case. First, a dense series of flexural cracks appeared at the bottom side of the beam, although their propagation was soon arrested by the high amount of steel reinforcement. Then, one of them turned into a shear crack, propagating towards the top side of the beam and pointing to the load application point (see Fig. 9). Immediately after, sub-horizontal cracks stemmed from the shear cracks at the bottom side of the beam and propagated towards the supports, driven by the dowel action. Finally, the collapse of the beam was determined by the explosive expulsion of a wedge-shaped portion in the compression region of the beam, just aside the load application point. As a result, the load-deflection response was

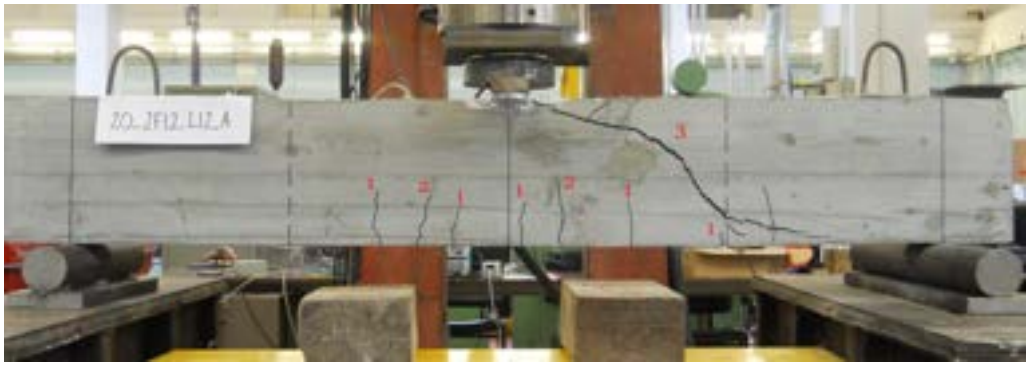


Figure 8: Picture of the beam H20_ρ1.13_S120-A after the test. Numbers 1 to 3 indicate the order of the cracks formation, as described in the text.

very brittle, being characterized by an almost linear-elastic branch up to the peak load, followed by a vertical drop in the load-carrying capacity (see Fig. 5d). In the context of failure transitions investigated in this work, the present behavior is identified as crushing failure. The critical crack paths for the three beams H20_ρ2.26_S120 are shown in Fig. 5d, while a picture taken after the test to specimen H20_ρ2.26_S120-B is shown in Fig. 9. It is interesting to note that in a case out of three two flexural cracks turned into shear cracks, almost symmetrically placed around the beam mid-span. They propagated in a competitive way, until one prevailed on the other, leading to the final collapse.



Figure 9: Picture of the beam H20_ρ2.26_S120-B after the test.

A further increase in the reinforcement amount to 3.39% did not produce variations on the overall mechanical behavior of the beams and on the crack pattern. The load-deflection curves and the trajectories of the critical cracks for specimens labeled

H20_ρ3.39_S120 are shown in Fig. 5e. They are very similar to those of the beams with $\rho = 2.26\%$ (see also the picture in Fig. 10).



Figure 10: Picture of the beam H20_ρ3.39_S120-C after the test.

3.2. Size effect

The set of beams tested to analyze the size effects with a constant reinforcement percentage, $\rho = 1.13\%$, is shown in Fig. 11. It is to be noted here that the smallest beam has a reinforcement ratio slightly lower than the others, being it equal to 1.00% because of practical reasons (see Tab. 1). However, due to the small difference, the results of the beams with $H = 0.05$m are included in this set, which allows to follow the transitions along the path (g)-(e)-(c) in Fig. 1. The load-deflection curves and the trajectories of the critical cracks are shown in Fig. 12. The smallest beams presented a quite large scatter in the overall mechanical response, as can be inferred from both the load vs. deflection curves and the crack patterns shown in Fig. 12a. One of the beams failed just after the attainment of the yield strain, another one presented a relatively small plastic phase, while the third one exhibited a well developed plastic phase. Such a scatter is probably due to the maximum dimension of aggregates that, being comparable to the beam height, had a serious influence on the development of the crack pattern, on the real properties of concrete and on the bond conditions of the reinforcement. The beams with H equal to 0.1 and 0.2 m exhibited a shear failure with a vertical drop in the load-carrying capacity after the peak load, except one of the beam 0.1 m high, which failed in bending with an extended plastic plateau (see Fig. 12b). The collapse of the largest beams, i.e., those with H equal to 0.4 and 0.8 m, was determined by crushing failure. The reinforcement

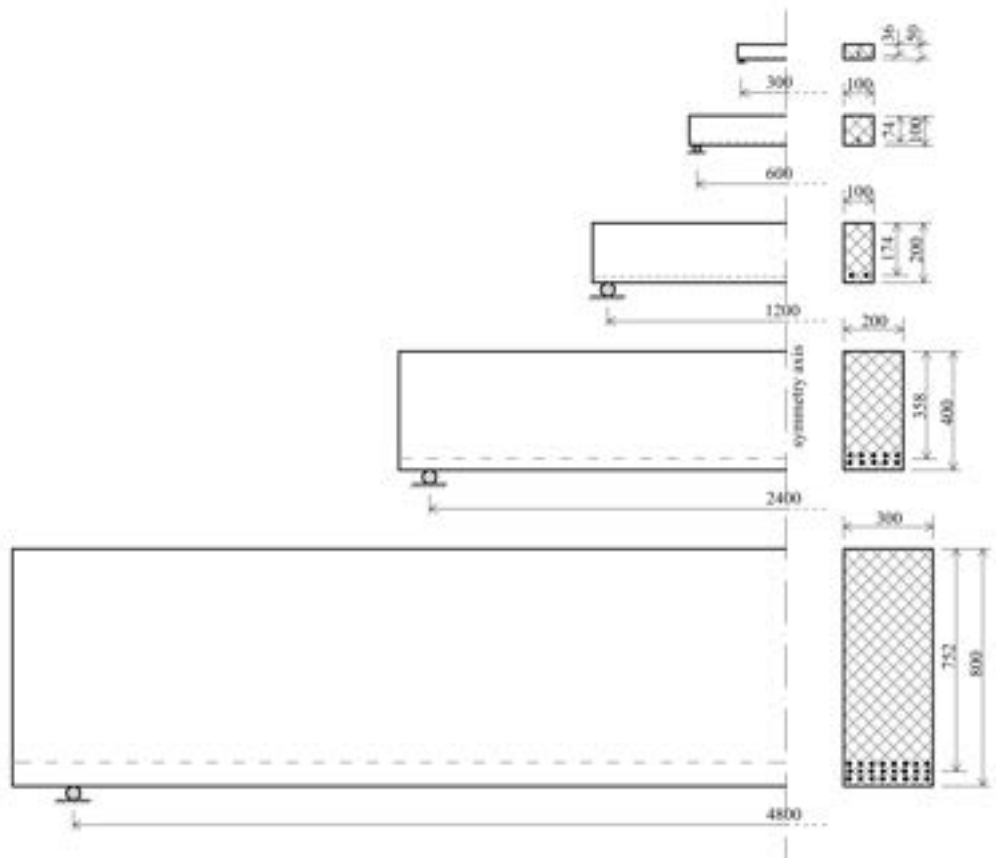


Figure 11: Set of beams used to analyze the size effect with constant reinforcement percentage $\rho = 1.13\%$.

yielding was obtained only for the smallest beam. In all the other cases, the collapse, both in shear and crushing mode, occurred before steel yielding. Given the interest the largest tested beams might arouse, a picture of the crack pattern obtained for one of the beam H40_ρ1.13_S240 and one of the beam H80_ρ1.13_S480 are shown in Fig. 13. Such pictures make evident how the crushing failure is determined by the spalling of a compressive wedge and its fracture by eccentric compression. Herein, it can be remarked that this failure mode can be delayed by adding stirrups or fibres reinforcement [9, 10, 6, 46]. More precisely, a correctly designed amount of stirrups counteract the formation of the critical shear crack, favoring the development of a more diffused crack pattern along the beam axis. The consistent resisting mechanism changes into a truss model, which consists of the longitudinal reinforcement, inclined concrete compression struts, stirrups,

and the compression chord. Accordingly, the design models provided by the Standards in case of stirrups reinforcement are different from those for beams without stirrups.

The size effects have been investigated also in the case of constant reinforcement area, $A_s = 226\,\mathrm{mm}^2$, path (i)-(e)-(a) in Fig. 1. Accordingly, by increasing the beam depth from 0.1 m to 0.8 m the reinforcement ratio decreases from 2.26% to 0.09% (see Fig. 14). The load-deflection curves and the trajectories of the critical cracks are shown in Fig. 15. Contrarily to the case with constant reinforcement ratio shown in Fig. 12, a transition from crushing to shear and flexural collapse is obtained by increasing the scale. The smallest beam, $H = 0.1$ m, exhibited a brittle behavior determined by a crushing collapse, the intermediate beam, $H = 0.2$ m, was characterized by a brittle behavior although due to a shear failure, whereas the two largest beams, $H = 0.4$ and 0.8 m, exhibited a ductile response, consequence of a flexural failure. In the case of $H = 0.8$ m and $\rho = 0.09\%$, the steel rebars yielded very early in the flexural crack and broke at the ultimate load. In this case (Fig. 15d), the cracking load equals the ultimate load.

3.3. Slenderness effect

The slenderness effect was analyzed by considering beams with a constant reinforcement ratio ρ=1.13%, a constant depth H=0.2 m and different beam spans varying from 0.6 m to 4.8 m (see Fig. 16). The results of the experimental tests are shown in Fig. 17. In the most stocky sample, having a shear slenderness $\lambda_l = 1.5$, an almost straight critical crack developed from the load application point to the support, typical of a strut-and-tie behavior. The ultimate load was reached for crushing of the compressed strut. By increasing the slenderness, the shape of the critical crack changed into that typical of a shear failure, for $\lambda_l = 3$, and of a flexural collapse, for $\lambda_l \geq 6$. Correspondingly, the load-deflection response became more and more ductile. A further increase of the slenderness does not provide any other transition between failure modes, the flexural failure remaining the proper one. On the other hand, a very high slenderness can amplify the effect of imperfections in the beam geometry and in the supporting and loading devices, giving rise to not negligible transversal bending and torsional moments in addition to the main action, i.e., the bending moment in the vertical plane. This phenomenon was made evident in the case of $\lambda_l = 12$ by the appearance of a lateral displacement and a twisting

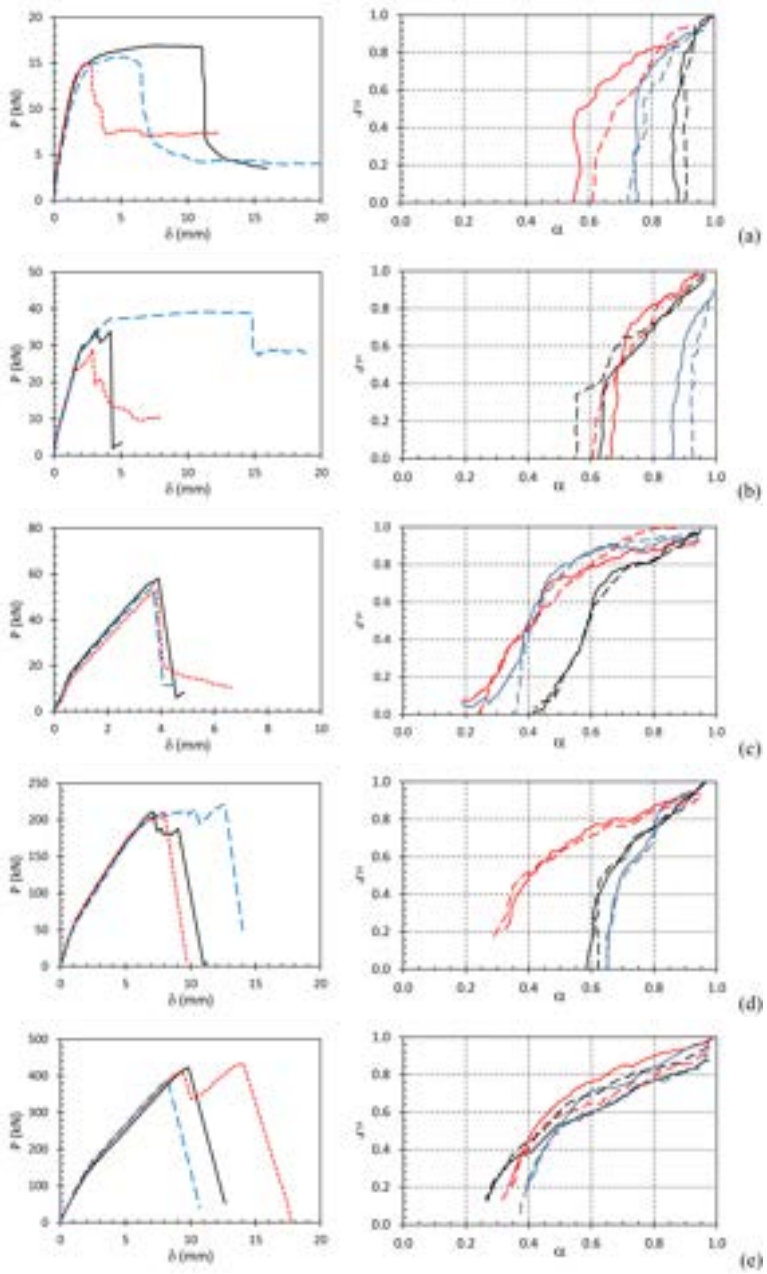


Figure 12: Load vs. mid-span deflection curves and critical crack trajectories for the series of beams designed to analyze the size effect with constant reinforcement percentage: (a) H05_ρ1.01_S030; (b) H10_ρ1.13_S060; (c) H20_ρ1.13_S120; (d) H40_ρ1.13_S240; (e) H80_ρ1.13_S480.



(a)

(b)

Figure 13: Pictures of the beams (a) H40_ρ1.13_S240-B and (b) H80_ρ1.13_S480-A after the test.

at the mid-span of the beam. Therefore, under such circumstances, the beam collapse was determined by the combined action of the three aforementioned solicitations.

The average value of the failure load and the failure mode for each beam type are reported in Tab. 4. In all the cases but one, the self-weight is not included being negligible compared to the applied force. In fact, the ratio between the shear force produced by the self-weight and the shear force produced by the applied load, evaluated at the critical section, i.e., in the position of the critical shear crack, is always lower than 1%. The only exception is the beam type H80_ρ0.09_S480. In that case, characterised by a flexural failure mode, the self-weight contributed to 15% of the total bending moment in the

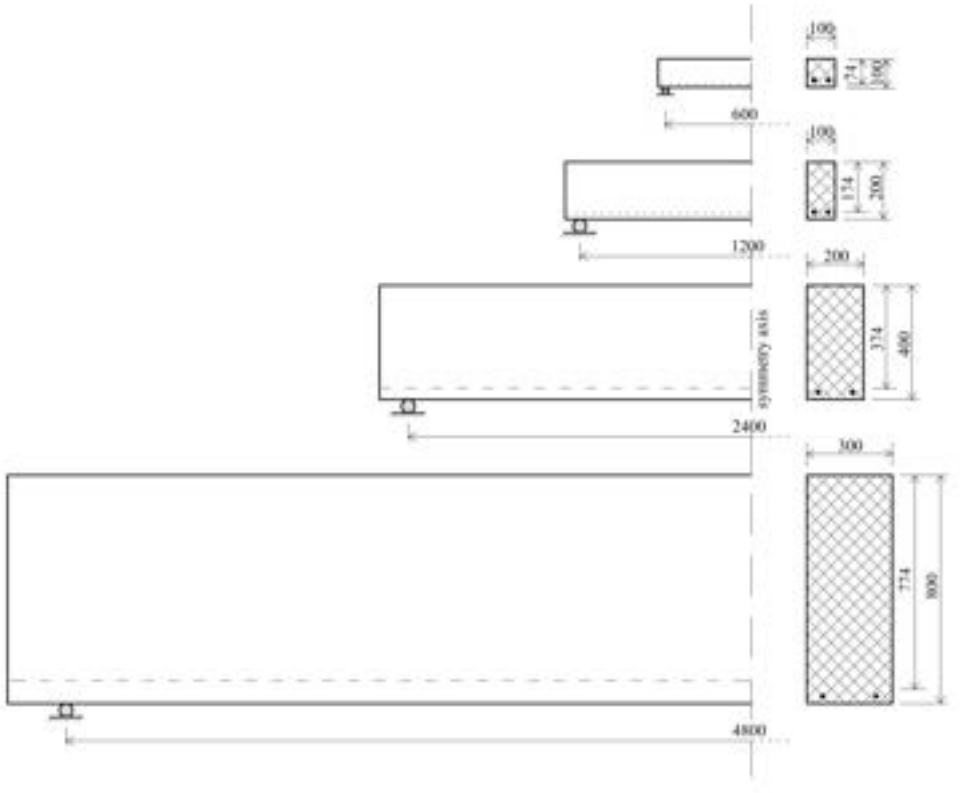


Figure 14: Set of beams used to analyze the size effect with constant reinforcement area, A_s.

mid-span. Accordingly, the concentrated load reported in Tab. 4 has been increased by 15 kN, which is the load that produces a bending moment in the mid-span section equal to that of the self-weight.

4. Comparison with Standards

The provisions of some codes of practice, namely Eurocode 2 [24], SIA 262 [63], and Model Code 2010 [64], were applied to calculate the failure loads of the tested beams. The formula provided by Eurocode 2 is of empirical derivation, the Swiss Code, SIA 262, provides an approach that is based on the Critical Shear Crack Model proposed by Muttoni et al. [16], and the Model Code 2010 provisions are based on the Simplified Modified Compression Field Theory [33].

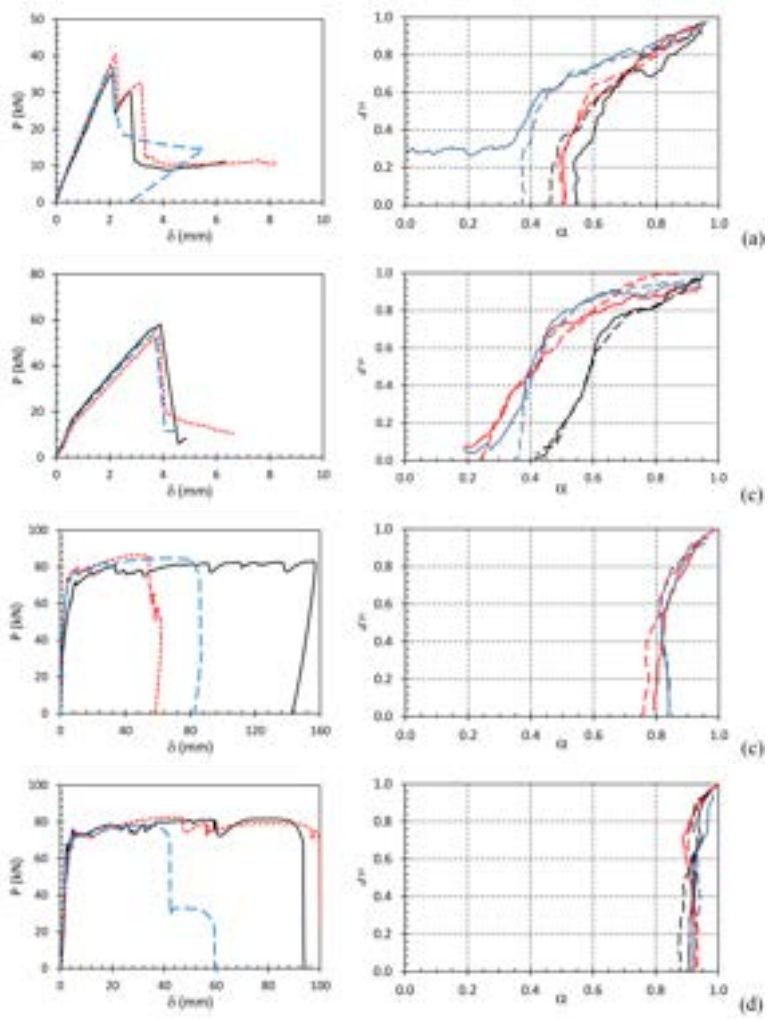


Figure 15: Load vs. mid-span deflection curves and critical crack trajectories for the series of beams designed to analyze the size effect with constant reinforcement area: (a) H10_ρ2.26_S060; (b) H20_ρ1.13_S120; (c) H40_ρ0.28_S240; (d) H80_ρ0.09_S480.

First, the resistant bending moment, M_{Rd}, and the resistant shear force, V_{Rd}, were computed for each of the beams by applying the codes provisions. Then, once M_{Rd} and V_{Rd} were calculated, the corresponding failure loads, $P(M_{Rd})$ and $P(V_{Rd})$, were computed taking into account the three-point bending setup, in the hypothesis of negligible self-weight effect. According to the design models, the load $P(M_{Rd})$ is associated to the flexural failure mode, whereas the design load $P(V_{Rd})$ is associated to the shear



Figure 16: Set of beams used to analyze the slenderness effect with constant reinforcement ratio.

and crushing failure modes. Finally, the real design load was taken, for each beam, as $\min\left[P(M_{Rd}); P(V_{Rd})\right]$.

As far as the resistant shear force is concerned, the following equation is provided by Eurocode 2 (units: MPa and mm):

$$V_{Rd} = \left[C_{Rd} k \left(100 \rho_l f_{ck}\right)^{1/3}\right] W d \tag{1}$$

where:

$$k = \min\left[1 + \sqrt{\frac{200}{d}}; 2.0\right] \tag{2}$$

is a coefficient taking into account the size effect,

$$\rho_l = \min\left[\frac{A_s}{W d}; 0.02\right] \tag{3}$$

is the longitudinal reinforcement ratio, f_{ck} is the characteristic value of the concrete compression strength, d is the effective beam depth, i.e., the distance of the extreme compression fiber to centroid of longitudinal reinforcement, W is the beam width, and the recommended value for C_{Rd} is $0.18/\gamma_c$, in which γ_c is the concrete partial safety

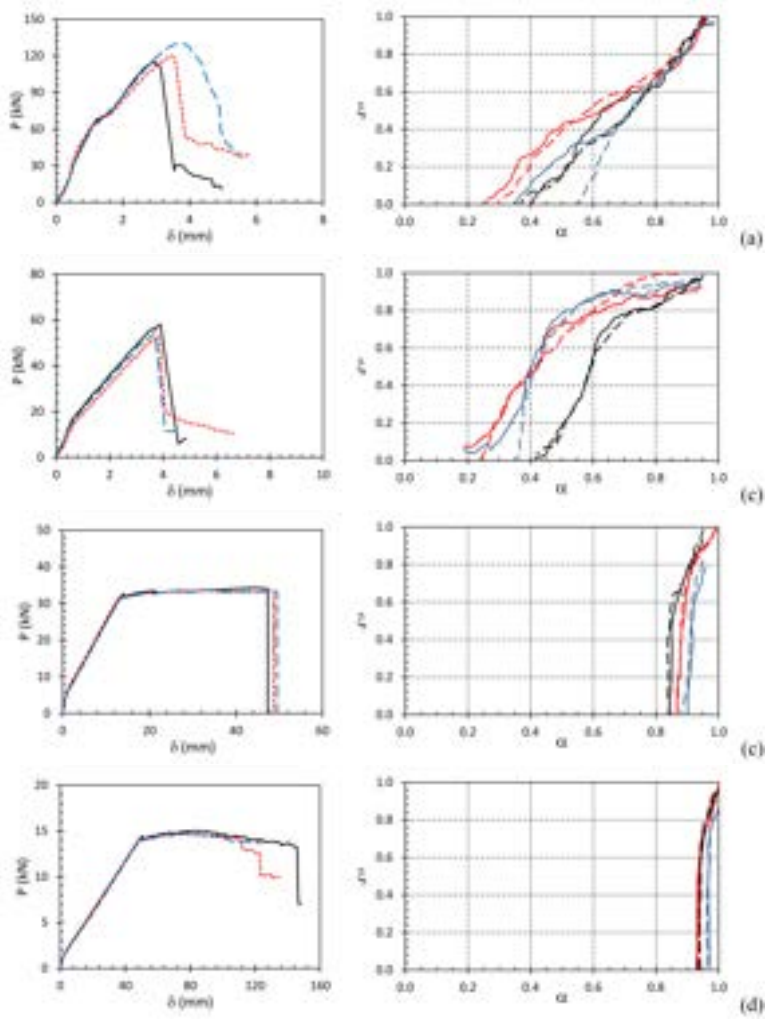


Figure 17: Load vs. mid-span deflection curves and critical crack trajectories for the series of beams designed to analyze the slenderness effect: (a) H20_ρ1.13_S060; (b) H20_ρ1.13_S120; (c) H20_ρ1.13_S240; (d) H20_ρ1.13_S480.

factor. It is to be noted that ρ_l is defined with respect to the effective beam depth, d, whereas ρ reported in Tab. 1 is defined with respect to the total beam depth, H.

The equation provided by SIA262 to compute the resistant shear force is (units: N and mm):

$$V_{Rd} = \frac{0.3 W d \sqrt{f_{ck}}}{\gamma_c \left(1 + \frac{50}{16+d_g} \frac{f_{yk}}{\gamma_s E_s} d \frac{m_{Ed}}{m_{Rd}}\right)} \tag{4}$$

Table 4: Dimensionless numbers, experimental peak loads and real failure mode for each type of beam.

Id. code	N_{P}	N_{C}	λ_l	$P_{exp}^{A,B,C}$ (kN)	Exp. failure mode
H20_ρ0.25_S120	0.25	7.91	3	17.64, 18.52, 17.80	flexural
H20_ρ0.50_S120	0.50	7.91	3	34.24, 35.96, 33.24	flexural/shear
H20_ρ1.13_S120	1.12	7.91	3	58.04, 52.68, 53.76	shear
H20_ρ2.26_S120	2.23	7.91	3	82.24, 70.20, 66.68	shear/crushing
H20_ρ3.39_S120	3.35	7.91	3	74.36, 75.76, 77.64	crushing
H05_ρ1.01_S030	0.50	3.95	3	16.92, 14.95, 15.68	flexural
H10_ρ1.13_S060	0.79	5.59	3	34.39, 28.90, 39.20	flexural/shear
H20_ρ1.13_S120	1.12	7.91	3	58.04, 52.68, 53.76	shear
H40_ρ1.13_S240	1.58	11.18	3	210.56, 211.42, 220.74	shear/crushing
H80_ρ1.13_S480	2.23	15.82	3	422.60, 432.92, 388.00	crushing
H10_ρ2.26_S060	1.58	5.59	3	35.43, 40.31, 37.02	shear/crushing
H20_ρ1.13_S120	1.12	7.91	3	58.04, 52.68, 53.76	shear
H40_ρ0.28_S240	0.40	11.18	3	82.89, 86.40, 84.66	flexural/shear
H80_ρ0.09_S480	0.19	15.82	3	81.56, 82.52, 78.16	flexural
H20_ρ1.13_S060	1.12	7.91	1.5	114.93, 119.90, 121.66	strut&tie
H20_ρ1.13_S120	1.12	7.91	3	58.04, 52.68, 53.76	shear
H20_ρ1.13_S240	1.12	7.91	6	34.26, 33.54, 33.58	flexural/shear
H20_ρ1.13_S480	1.12	7.91	12	15.00, 14.72, 14.76	flexural

where: d_g is the maximum aggregate size, γ_s is the steel partial safety factor, f_{yk} is the characteristic value of the steel yielding strength, m_{Ed} and m_{Rd} are the applied and the resistant bending moment in the critical section of the beam, respectively. The position of the critical section depends on the load configuration. In the case of concentrated forces, the critical section is $d/2$ from the application of the load (see ref. [16] for more details).

The equation provided by Model Code 2010 to determine the resistant shear force is

(units: N and mm):

$$V_{Rd} = k_v \frac{\sqrt{f_{ck}}}{\gamma_c} zW \tag{5}$$

where:

$$k_v = \frac{0.4}{1 + 1500\varepsilon_x} \frac{1300}{1000 + k_{dg} z}, \tag{6}$$

k_{dg} is a coefficient taking into account the maximum aggregate size, ε_x is the longitudinal strain at the mid-depth of the effective shear depth in the control section, and z is the effective shear depth, taken equal to $0.9d$. Even though the correct evaluation of the longitudinal strain ε_x requires the adoption of an iterative procedure, its value was computed by applying Eq. (7.3.16) of Model Code 2010, as also suggested in [65].

The resistant bending moment was evaluated in the same way for all the three Standards, on the basis of the steel yielding strength, f_{yk}. In order for a more direct comparison with the experimental results, the partial safety factors for concrete and steel were assumed equal to 1.0. Besides, the average values of the material strengths were used instead of the characteristic ones. All the geometrical and mechanical parameters needed to compute the design loads according to the considered Standards can be taken from Tabs. 1, 2, and 3, and from Figs. 4, 11, 14, 16.

The failure mode and load carrying capacity predicted by the three considered Standards for each of the beam type are reported in Tab. **??**, together with the corresponding average values of the ultimate load obtained with the experimental tests. It is worth noticing that the failure mode identified as crushing in the present study does not have a specific design formula in the Standards. It is treated as a shear failure. The comparison between Standards predictions and experimental results is then shown in Fig. 18 in terms of experimental failure load to design load ratio, P_{exp}/P_{design}, where P_{exp} is the average value between the three results obtained for each beam type. In the diagrams, not filled-in markers identify cases in which the design failure load is determined by the resistant bending moment, i.e., $P(M_{Rd}) < P(V_{Rd})$, whereas filled-in markers identify cases characterized by $P(V_{Rd}) < P(M_{Rd})$.

In Fig. 18a the ratio P_{exp}/P_{design} is shown as a function of the reinforcement percentage for the beams belonging to the first series of specimens listed in Tab. 1. The predictions of the three codes are coincident for the flexural failure mode. In this case, there is an intrinsic safety factor of about 1.25, which is due to the difference between the

Average value of the experimental peak loads reported in Tab.4 and failure mode and load carrying capacity predicted by the three Standards: EC2, SIA262 and MC2010. (f) stands for predicted flexural failure ($P(M_{Rd}) < P(V_{Rd})$), (s) stands for predicted shear failure ($P(V_{Rd}) < P(M_{Rd})$).

Id. code	P_{exp}^{ave} (kN)	P_{EC2} (kN)	P_{SIA262} (kN)	P_{MC2010} (kN)
H20_ρ0.25_S120	17.99	14.47 (f)	14.47 (f)	14.47 (f)
H20_ρ0.50_S120	34.38	28.41 (f)	28.41 (f)	24.89 (s)
H20_ρ1.13_S120	54.83	46.75 (s)	44.06 (s)	31.20 (s)
H20_ρ2.26_S120	73.04	49.02 (s)	43.58 (s)	34.91 (s)
H20_ρ3.39_S120	75.92	49.02 (s)	46.36 (s)	42.47 (s)
H05_ρ1.01_S030	15.85	10.30 (s)	10.98 (f)	5.25 (s)
H10_ρ1.13_S060	34.16	20.98 (s)	21.28 (s)	11.07 (s)
H20_ρ1.13_S120	54.83	46.75 (s)	44.06 (s)	31.20 (s)
H40_ρ1.13_S240	214.24	166.49 (s)	137.96 (s)	117.37 (s)
H80_ρ1.13_S480	414.51	447.64 (s)	382.16 (s)	394.12 (s)
H10_ρ2.26_S060	37.59	22.96 (s)	23.46 (s)	16.51 (s)
H20_ρ1.13_S120	54.83	46.75 (s)	44.06 (s)	31.20 (s)
H40_ρ0.28_S240	84.65	69.13 (f)	69.13 (f)	69.13 (f)
H80_ρ0.09_S480	94.75	72.49 (f)	72.49 (f)	72.49 (f)
H20_ρ1.13_S060	121.66	46.75 (s)	43.73 (s)	27.20 (s)
H20_ρ1.13_S120	54.83	46.75 (s)	44.06 (s)	31.20 (s)
H20_ρ1.13_S240	33.79	30.06 (f)	30.06 (f)	28.10 (s)
H20_ρ1.13_S480	14.83	15.03 (f)	15.03 (f)	15.03 (f)

ultimate and the yielding strength of the steel reinforcement. Concerning the evaluation of the resistant shear load, EC 2 and SIA 262 provide quite similar results, whereas the predictions of MC 2010 are more conservative. In general, the intrinsic safety factor increases by increasing the reinforcement percentage.

The ratio P_{exp}/P_{design} for the second series of beams listed in Tab. 1 is shown in

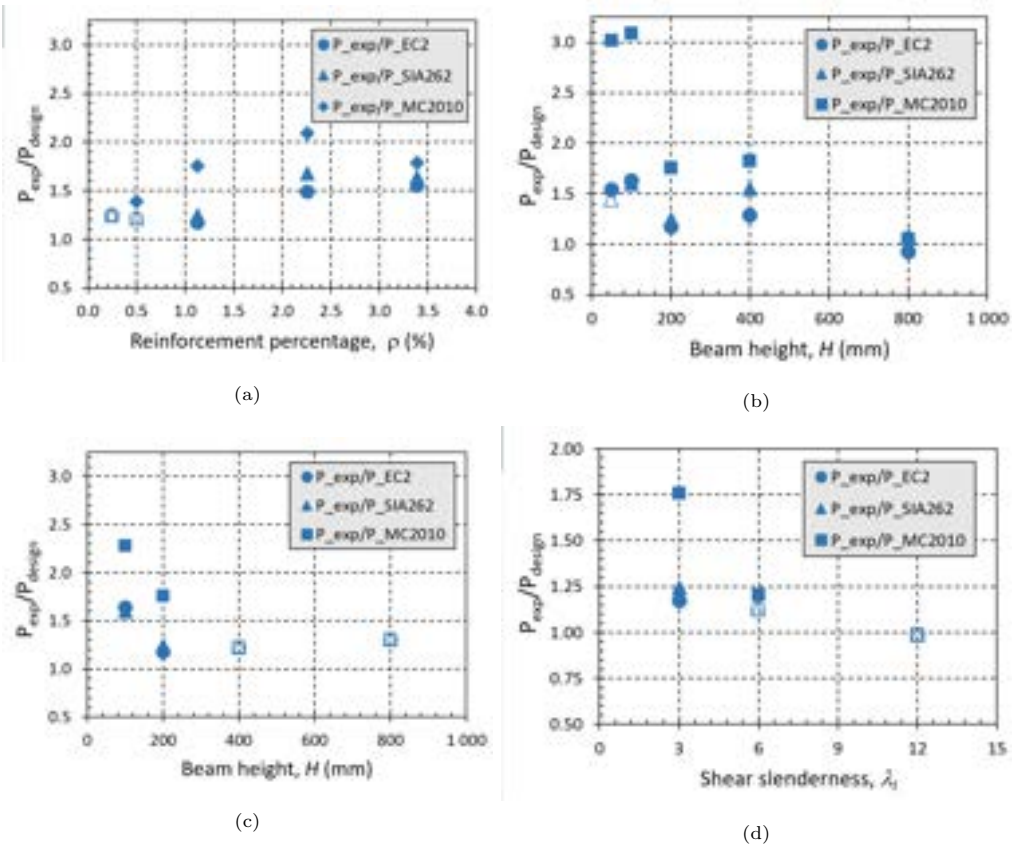


Figure 18: Comparison between the failure loads predicted by codes of practice and the experimental results: (a) effect of the reinforcement ratio; (b) and (c) effect of the structural scale with constant reinforcement percentage and reinforcement area, respectively; (d) effect of the slenderness.

Fig. 18b as a function of the beam depth. EC 2 and MC 2010 predict shear failure for all the beams included in this series, whereas SIA 262 predicts flexural failure for $H = 0.05$ m. The predictions of EC 2 and SIA 262 are close to each other, whereas those of MC 2010 are more conservative, especially for the two smallest beams, which show a safety factor of about 3.0. However, from the safety stand point, the most striking result is the decrease of the intrinsic safety factor by increasing the structural scale. In the case of $H = 0.8$ the safety factor drops to about 1.0 for all the three considered codes.

The ratio P_{exp}/P_{design} for the third series of beams listed in Tab. 1 is shown in Fig. 18c as a function of the beam depth. According to the experimental results, all

the three codes predict shear failure for $H = 0.1, 0.2$ m, and flexural failure for $H = 0.4, 0.8$ m. The increase in the structural scale, therefore, is no longer a concern for the structural safety because of the dominance of the flexural failure at large scales. On the contrary, a decrease in the structural scale evidences an underestimation of the real shear capacity, especially for MC 2010, with an intrinsic safety factor that increases up to 2.3 for $H = 0.1$ m.

Finally, the ratio P_{exp}/P_{design} for the forth series of beams listed in Tab. 1 is shown in Fig. 18d as a function of the shear slenderness. The result of the shortest beam was not included because of its strut-and-tie behaviour that is not encompassed by the considered design models. The decrease in the safety factor to 1.0 for a slenderness equal to 12 is due to the concomitant effect of the transverse bending moment and twisting moment discussed in Section 3.3.

5. Discussion

5.1. Nondimensional analysis

Recent studies by the present authors [17, 48, 54] have shown that the failure mode transitions in RC beams can be conveniently analyzed on the basis of three dimensionless parameters, namely the shear slenderness, λ_l, and two brittleness numbers, N_P and N_C, obtained by applying the Buckingham's Π-theorem of dimensional analysis to the functional relationship among the geometrical and mechanical parameters involved in the mechanical problem. The procedure yields to the combination of the independent quantities into a reduced amount of dimensionless variables (see [37, 66, 17] for more details on the application of the procedure):

$$N_P = \rho \frac{f_y H^{0.5}}{K_{IC}} \tag{7}$$

introduced by Carpinteri since 1981 [36], and

$$N_C = \frac{f_c H^{0.5}}{K_{IC}} \tag{8}$$

introduced by Carpinteri et al. in [17]. The dimensional analysis procedure applied to derive N_P and N_C provides also the expression for the consistent normalized load, which

reads:

$$\tilde{P} = \frac{P}{K_{IC} H^{0.5} W} \tag{9}$$

In Eqs. 7, 8 and 9, K_{IC} is the concrete fracture toughness, which has been herein computed by means of the fundamental Irwin's relation, holding in the framework of linear elastic fracture mechanics:

$$K_{IC} = \sqrt{E_c G_F} \tag{10}$$

N_P includes the effects of the reinforcement amount and strength, the concrete toughness and the structural scale, whereas N_C introduces the effect of the concrete compression strength. In dimensionless terms, the structural response is expected to be only function of the three dimensionless numbers. In particular, physical similarity is predicted when the three dimensionless parameters are kept constant, although the single mechanical and geometrical properties vary [17, 66, 55].

The values of the three dimensionless numbers are reported in Tab. 4 for all the beam types tested in the experimental program. It is worth noting that in the first three series of beams λ_l is constant while N_C varies because of the variation in the beam depth, H. Since the effect of the structural scale is also taken into account by N_P, N_C does not add any information with respect to N_P. Therefore, the results of the first three series of specimens can be analysed as a function of N_P only. This is not possible in case the concrete strength varies, since f_c is included only in the parameter N_C. The average values of the dimensionless failure loads for the first three series of specimens are shown in Fig. 19 as functions of N_P. The results, apparently uncorrelated one from another, identify a clear trend as a function of N_P. Three regions can be identified in terms of failure mode: flexural failure for $N_P \lesssim 0.7$, shear failure for $0.7 \lesssim N_P \lesssim 2.0$, and crushing failure for $N_P \gtrsim 2.0$. As a first approximation, the $\tilde{P} - N_P$ relationship can be described by a tri-lateral function, as shown in Fig. 19. The decrease in the slope of the $\tilde{P} - N_P$ linear functions up to an almost horizontal line in the region of crushing collapse is consistent with the theoretical results obtained by Carpinteri and co-authors by applying a bridged crack model based approach (see Fig. 10 in ref. [17]).

The effect of the slenderness is analysed separately in Fig. 20. In this figure, the values of N_P for the fourth series of beams are reported as a function of λ_l. According to the results of the study carried out by Carpinteri and co-workers [17] the N_P vs. λ_l plan is

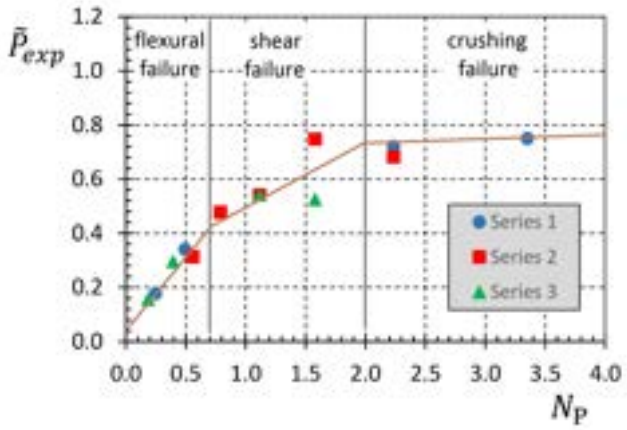


Figure 19: Dimensionless failure loads for the first three series of beams (see Tab. 1) as a function of the brittleness number N_P.

435 subdivided in two failure domains, namely flexural and shear. The curve separating the two domains can be obtained by running the numerical approach based on the bridged crack model presented in ref. [17]. It is drawn in Fig. 20, confirming that the parameters of the fourth set of beams were selected to capture the transition between flexural and shear failure modes.

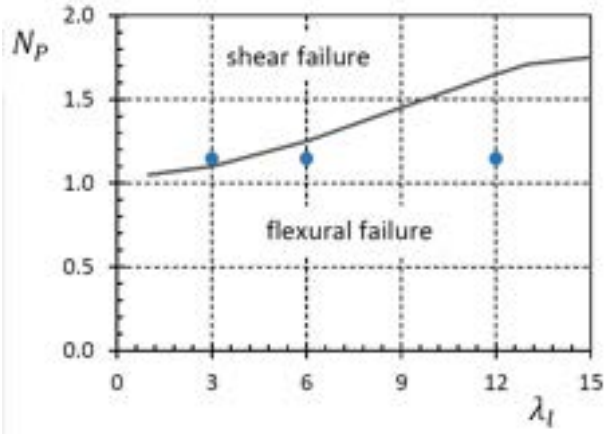
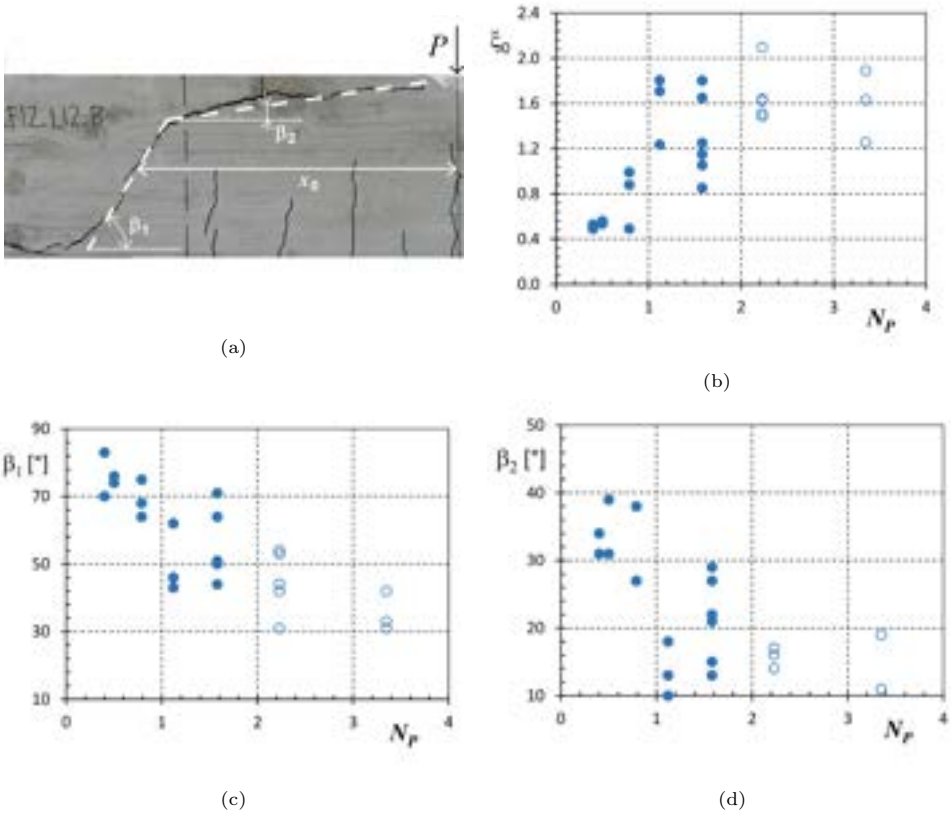


Figure 20: Transition from flexural to shear failure by varying N_P and λ_l according to the experimental results of the fourth series of beams listed in Tab. 1.

5.2. Critical shear crack

From the analysis of the models proposed in the literature [16, 17, 63, 67, 64], it emerges the importance of knowing the correct position and shape of the critical crack for an accurate prediction of the shear capacity. The shape of the critical cracks obtained in the experimental tests is herein analysed in a simplified way, by approximating the cracks with a bi-lateral path, as sketched in Fig. 21a. In particular, the two branches of the bilateral shape assumed to interpolate the critical shear crack have been obtained by linear regression. The data points included in the regression are those placed between the level of the longitudinal reinforcement and the upper side of the beam, while different positions for the knee formed by the two straight lines have been tried, to minimize the error. According to such a schematic, the path of the critical crack can be described by three parameters: the distance of the crack from the load application point, $\xi_0 = x_0/H$, evaluated at the mid-height of the beam, the inclination of the first branch, β_1, and the inclination of the second branch, β_2. The values of the three parameters obtained from the beams failed by shear or crushing are reported in Tab. 5 and shown in Fig. 21b-d as a function of N_P.

The parameter ξ_0 increases from 0.4 up to 2.0 for N_P varying from 0.5 to 3.4. Such a result evidences that, in the case of concentrated loads, the position of the control section defined by SIA 262 and Model Code 2010, i.e., the position of the critical crack, does not depend only on the load configuration but also on the geometrical and mechanical properties of the beam. Simultaneously, β_1 decreases from 80° to 30°, and β_2 decreases from 40° to 10°. The decrease in β_1 is almost linear, while the decrease of β_2 is faster for low values of N_P. According to the mechanical models behind the provisions of Model Code 2010 and SIA 262, the increase of ξ_0 with N_P is beneficial for the shear strength because it means that the critical crack, i.e. the control section in the models, moves towards regions subjected to lower values of bending moment. On the contrary, the decrease in β_1 is detrimental because it reduces the contribution of the aggregate interlocking to the shear strength. Analogously, the concomitant increase in ξ_0 and decrease in β_2 is harmful because it reduces the thickness of the compressed chord located above the critical shear crack, making it more prone to the buckling collapse observed in the cases classified as crushing failure mode in the present study. In the experimental



(a)

(b)

(c)

(d)

Figure 21: Critical crack: (a) simplified representation of the path; (b) position of the crack, (c) slope of the first branch and (d) slope of the second branch as a function of N_P, for $\lambda_l = 3$. Filled-in markers refer to shear failure, empty markers to crushing failure.

Table 5: Geometrical parameters of the critical cracks: position, $\xi_0 = x_0/H$, slope of the first branch, β_1, and slope of the second branch, β_2.

Id. code	N_{P}	ξ_0	β_1 [deg]	β_2 [deg]
H20_ρ0.50_S120-B,C	0.50	0.54, 0.56	76, 74	39, 31
H20_ρ1.13_S120-A,B,C	1.12	1.24, 1.81, 1.71	46, 43, 62	18, 13, 10
H20_ρ2.26_S120-A,B,C	2.23	2.10, 1.63, 1.49	54, 53, 42	9, 14, 17
H20_ρ3.39_S120-A,B,C	3.35	1.26, 1.89, 1.63	42, 33, 31	19, 11, 11
H10_ρ1.13_S060-A,B,C	0.79	0.99, 0.88, 0.49	64, 68, 75	27, 27, 38
H20_ρ1.13_S120-A,B,C	1.12	1.24, 1.81, 1.71	46, 43, 62	18, 13, 10
H40_ρ1.13_S240-A,B,C	1.58	1.06, 1.80, 0.85	71, 50, 64	27, 15, 29
H80_ρ1.13_S480-A,B,C	2.23	1.63, 1.64, 1.51	31, 44, 44	16, 14, 17
H10_ρ2.26_S060-A,B,C	1.58	1.15, 1.25, 1.65	44, 51, 50	21, 22, 13
H20_ρ1.13_S120-A,B,C	1.12	1.24, 1.81, 1.71	46, 43, 62	18, 13, 10
H40_ρ0.28_S240-B,C	0.40	0.53, 0.49	70, 83	34, 31

tests, the latter phenomenon was particularly evident for the largest beams of the second series of specimens, namely H80_ρ1.13_S480, which, in fact, exhibited a very brittle failure due to concrete crushing.

6. Conclusions

The contributions brought by the present paper to the study of the shear strength in RC members without transverse reinforcement are manifold. The following main conclusions can be drawn.

- The global failure mode transition scheme theoretically introduced by Carpinteri and co-workers has been confirmed by the results of the experimental tests. All the transition paths included in this scheme were investigated experimentally and analyzed in terms of failure load and critical crack pattern.

- The use of the dimensionless numbers N_P, N_C and λ_l in the analysis of the results

as clear advantages compared to the use of the single parameters. The experimental results herein presented are a valuable contribution for the estimation of the values of the brittleness numbers that identify the flexural to shear to crushing failure transitions.

- Concerning the provisions of Eurocode 2, Model Code 2010 and SIA 262 for the failure load of RC members without transversal reinforcement, the experimental results herein reported pinpointed that the effect of the reinforcement amount is properly taken into account, whereas improvements are still required for a correct prediction of the size effect. This is made clear by analysing the safety factor defined as the ratio between experimental and predicted failure load, which is very large for low beam depths, even larger than 2.0 in case the Model Code 2010 is applied, whereas it dangerously decreases to about 1.0 for the beam 0.8 m high.

- The large underestimation of the shear strength provided by Model Code 2010 for some of the cases is due to the dependence of the shear strength on the values of bending moment and shear force acting in the control section. In that regard, the three-point bending setup is the most unfavorable scheme, since it maximizes both the bending moment and the shear force in the mid-span cross section whereas, for example, the simply supported beam subjected to a distributed load maximizes the shear force on the supports and the bending moment at the mid-span. The effect of the structural scheme is not included in the formula by Eurocode 2, whereas it seems to be more appropriately taken into account in the formula by SIA 262.

- Codes predictions may be improved by taking into account the variation in position and shape of the critical crack as a function of the main parameters of the problem. For that purpose, the main features of the critical crack have been reported as a function of the brittleness number N_P. Pretty clear trends have been obtained.

Finally, the results of the experimental program herein presented, which is unique in the recent literature for number of tested specimens and variety of parameters investigated, constitute a comprehensive database useful for future investigations.

CRediT author statement

M. Corrado: Investigation, Formal Analysis, Writing - Original Draft. **G. Ventura:** Methodology, Investigation, Writing - Review & Editing. **A. Carpinteri:** Conceptualization, Supervision, Funding Acquisition.

References

[1] W. A. Slater, A. R. Lord, R. R. Zipprodt, Shear tests of reinforced concrete beams, in: Technological Papers of the Bureau of Standards, No. 314, US Government Printing Office, 1926, pp. 385–495.

[2] T. Shioya, Shear properties of large reinforced concrete members, in: Special Report of Institute of Technology, No. 25, Shimizu Corp., 1989.

[3] M. V. Kani, M. W. Huggins, R. R. Wittkopp, Kani on Shear in Reinforced Concrete, University of Toronto Press, Toronto, 1979.

[4] Z. P. Bažant, M. P. Kazemi, Size effect in diagonal shear failure, ACI Structural Journal 88 (3) (1991) 268–276.

[5] G. Konig, R. Grimm, G. Remmel, Shear behaviour of longitudinally reinforced concrete members of hsc, Darmstadt Concrete 8 (1993) 27–42.

[6] A. Koray Tureyen, R. J. Frosch, Shear tests of frp-reinforced concrete beams without stirrups, ACI Structural Journal 99 (2002) 427–434.

[7] J. Suchorzewski, E. Korol, J. Tejchman, Z. Mróz, Experimental study of shear strength and failure mechanisms in rc beams scaled along height or length, Engineering Structures 157 (2018) 203–223.

[8] M. P. Collins, E. C. Bentz, E. G. Sherwood, Where is shear reinforcement required? review of research results and design procedures, ACI Structural Journal 105 (2008) 590–600.

[9] M. Khuntia, B. Stojadinovi, S. C. Goel, Shear strength of normal and high-strength fiber reinforced concrete beams without stirrups, ACI Structural Journal 96 (1999) 282–289.

[10] Y.-K. Kwat, M. O. Eberhard, W.-S. Kim, J. Kim, Shear strength of steel fiber-reinforced concrete beams without stirrups, ACI Structural Journal 99 (2002) 530–538.

[11] A. Lubell, T. Sherwood, E. C. Bentz, M. P. Collins, Safe shear design of large, wide beams, Concrete International ?? (2004) 67–78.

[12] E. C. Bentz, Empirical modeling of reinforced concrete shear strength size effect for members without stirrups, ACI Structural Journal 102 (2005) 232–241.

[13] L. Yu, Y. Che, Y. Song, Shear behavior of large reinforced concrete beams without web reinforcement, Advances in Structural Engineering 16 (4) (2013) 653–665.

[14] G. Russo, G. Somma, D. Mitri, Shear strength analysis and prediction for reinforced concrete beams without stirrups, ASCE Journal of Structural Engineering 131 (2005) 66–74.

[15] M. P. Collins, E. C. Bentz, E. G. Sherwood, L. Xie, An adequate theory for the shear strength of reinforced concrete structures, Magazine of Concrete Research 60 (2008) 635–650.

[16] A. Muttoni, M. Fernández Ruiz, Shear strength of members without transverse reinforcement as function of critical shear crack width, ACI Structural Journal 2 (ARTICLE).

[17] A. Carpinteri, J. R. Carmona, G. Ventura, Failure mode transitions in reinforced concrete beams-part 1: Theoretical model, ACI Structural Journal 108 (3) (2011) 277–285.

[18] X. An, K. Maekawa, H. Okamura, Numerical simulation of size effect in shear strength of rc beams, Doboku Gakkai Ronbunshu 1997 (564) (1997) 297–316.

[19] A. H. Gandomi, D. Mohammadzadeh, J. L. Pérez-Ordóñez, A. H. Alavi, Linear genetic programming for shear strength prediction of reinforced concrete beams without stirrups, Applied Soft Computing 19 (2014) 112–120.

[20] A. Fiore, G. Quaranta, G. C. Marano, G. Monti, Evolutionary polynomial regression-based statistical determination of the shear capacity equation for reinforced concrete beams without stirrups, ASCE Journal of Computing in Civil Engineering 30 (2016) 04014111.

[21] ACI 318-14: Building code requirements for structural concrete, American Concrete Institute, 1999.

[22] ACI 224R-01: Control of cracking in concrete structures, American Concrete Institute-ACI, 2001.

[23] ACI 435R-95: Control of deflection in concrete structures, American Concrete Institute-ACI, 2000.

[24] Eurocode 2, EN 1992-1-1: Design of Concrete Structures: General Rules and Rules for Buildings, European Committee for Standardization, 2004.

[25] Z. P. Bažant, J. Planas, Fracture Size Effect in Concrete and Other Quasibrittle Materials, CRC Press, Boca Raton, 1998.

[26] Z. P. Bažant, Size effect in blunt fracture: Concrete, rock, metal, Journal of Engineering Mechanics-ASCE 110 (1984) 518–535.

[27] Z. P. Bažant, P. R. Pffeifer, Shear fracture test of concrete, Materials and Structures 19 (1986) 111–121.

[28] Z. P. Bažant, Q. Yu, Designing against size effect on shear strength of reinforced concrete beams without stirrups: I. Formulation, Journal of Structural Engineering-ASCE 131 (12) (2005) 1877–1885.

[29] Z. P. Bažant, Q. Yu, Designing against size effect on shear strength of reinforced concrete beams without stirrups: II. Verification and calibration, Journal of Structural Engineering-ASCE 131 (12) (2005) 1886–1897.

[30] Z. P. Bažant, Size effect in tensile and compression fracture of concrete structures: Computational modeling and desing, in: Fracture Mechanics of Concrete Structures, F.H. Wittmann, Ed., Aedificatio Publishers, Freiburg, Germany, 1998, pp. 1905–1922.

[31] Z. P. Bazant, J.-K. Kim, Size effect in shear failure of longitudinally reinforced beams., Journal of the American Concrete Institute 81 (5) (1984) 456–468.

[32] F. J. Vecchio, M. P. Collins, The modified compression-field theory for reinforced concrete elements subjected to shear, ACI Journal 105 (1986) 219–231.

[33] E. C. Bentz, F. J. Vecchio, M. P. Collins, The simplified mcft for calculating the shear strength of reinforced concrete elements, ACI Structural Journal 103 (2006) 614–624.

[34] A. Muttoni, J. Schwartz, Behavior of beams and punching in slabs without shear reinforcement, in:

IABSE colloquium, Vol. 62, IABSE Colloquium, 1991, pp. 703–708.

[35] M. Fernández Ruiz, A. Muttoni, On development of suitable stress fields for structural concrete, ACI Structural Journal 104 (2007) 495–502.

[36] A. Carpinteri, A fracture mechanics model for reinforced concrete collapse, in: IABSE colloquium on Advanced Mechanics of Reinforced Concrete, Delft, The Netherlands, 1981, pp. 17–30.

[37] A. Carpinteri, Stability of fracturing process in RC beams, Journal of Structural Engineering-ASCE 110 (1984) 544–558.

[38] C. Bosco, A. Carpinteri, P. G. Debernardi, Fracture of reinforced concrete: Scale effect and snap-back instability, Engineering Fracture Mechanics 35 (4-5) (1990) 228–236.

[39] C. Bosco, A. Carpinteri, P. G. Debernardi, Minimum reinforcement in high-strength concrete, Journal of Structural Engineering -ASCE 116 (2) (1990) 228–236.

[40] C. Bosco, A. Carpinteri, Fracture mechanics evaluation of minimum reinforcement in concrete structures, in: A. Carpinteri (Ed.), Application of Fracture Mechanics to Reinforced Concrete, Elsevier, London, 1992, pp. 347–377.

[41] A. Carpinteri, Ed., Minimum Reinforcement in Concrete Members, Number 24 in ESIS Publications. Elsevier, London, 1999.

[42] A. Carpinteri, B. Chiaia, G. Ferro, Size effect on nominal tensile strength of concrete structures: Multifractality of material ligaments and dimensional transition from order to disorder, Materials and Structures 28 (1998) 311–317.

[43] M. Corrado, E. Cadamuro, A. Carpinteri, Dimensional analysis approach to study snap back-to-softening-to-ductile transitions in lightly reinforced quasi-brittle materials, International journal of fracture 172 (1) (2011) 53–63.

[44] A. Carpinteri, R. Massabò, Continous vs. Discontinous bridged-crack model for fiber reinforced materials in flexure, International Journal of Solids and Structures 34 (21) (1997) 2321–2338.

[45] A. Carpinteri, G. Ferro, G. Ventura, Size effects on flexural response of reinforced concrete elements with a nonlinear matrix, Engineering Fracture Mechanics 70 (2003) 995–1013.

[46] A. Carpinteri, E. Cadamuro, G. Ventura, Fiber-reinforced concrete in flexure: a cohesive/overlapping crack model application, Materials and Structures 48 (1-2) (2015) 235–247.

[47] A. Carpinteri, J. R. Carmona, G. Ventura, Propagation of flexural and shear cracks through reinforced concrete beams by the bridged crack model, Magazine of Concrete Reseach 59 (10) (2007) 743–756.

[48] A. Carpinteri, J. R. Carmona, G. Ventura, Failure mode transitions in reinforced concrete beams–part 2: Experimental tests, ACI Structural Journal 108 (3) (2011) 286–293.

[49] A. Carpinteri, M. Corrado, G. Mancini, M. Paggi, Size-scale effects on plastic rotational capacity of reinforced concrete beams., ACI structural journal 106 (6) (2009) 887–896.

[50] A. Carpinteri, M. Corrado, G. Goso, M. Paggi, Size-scale effects on interaction diagrams for reinforced concrete columns, Construction and Building Materials 27 (1) (2012) 271–279.

[51] M. Fernández Ruiz, A. Muttoni, Applications of the critical shear crack theory to punching of r/c slabs with transverse reinforcement, ACI Structural Journal 106 (ARTICLE).

[52] A. Muttoni, Punching shear strength of reinforced concrete slabs without transverse reinforcement, ACI structural Journal 105 (2008) 440–450.

[53] A. Carpinteri, G. Ventura, J. Carmona, Flexural to shear and crushing failure transitions in rc beams by the bridged crack model, in: Fracture mechanics of concrete structures. Proceedings of the 6th International FraMCoS Conference, Catania, Italy, Vol. 2, 2007, pp. 677–684.

[54] A. Carpinteri, M. Corrado, G. Ventura, Failure mode scaling transitions in rc beams in flexure: tensile, shearing, crushing, in: Proceedings of the 8th international conference on fracture mechanics of concrete and concrete structures, Toledo, Spain, Vol. 31, 2013, pp. 31–43.

[55] A. Carpinteri, M. Corrado, Upper and lower bounds for structural design of rc members with ductile response, Engineering Structures 33 (2011) 3432–3441.

[56] CEN, EN 12350-2:2009 Testing fresh concrete - Part 2: Slump test, Brussels: European Committee for Standardization, 2009.

[57] CEN, EN 206-1:2013 Concrete - Part 1: Specification, performance, production and conformity, Brussels: European Committee for Standardization, 2013.

[58] CEN, EN 12390-3:2009 Testing hardened concrete - Part 3: Compressive strength of test specimens, Brussels: European Committee for Standardization, 2009.

[59] UNI, UNI 6556: Determinazione del modulo elastico secante a compressione, Ente Nazionale Italiano di Unificazione, 1976.

[60] RILEM TCS, Determination of the fracture energy of mortar and concrete by means of three-point bend tests on notched beams, Materials and Structures 18 (1985) 285–290.

[61] CEN, EN ISO 15630-1:2010 Steel for reinforcement and prestressing of concrete - Test methods - Part 1: Reinforcing bars, wire rod and wire, Brussels: European Committee for Standardization, 2010.

[62] CEN, EN ISO 6892-1:2009 Metallic materials - Tensile testing - Part 1: Method of test at room temperature, Brussels: European Committee for Standardization, 2009.

[63] SIA 262, SIA Code 262 for Concrete Structures, Swiss Society of Engineers and Architects, 2003.

[64] International Federation for Structural Concrete, fib Model Code for Concrete Structures 2010, Ernst & Sohn, 2010.

[65] V. Sigrist, E. Bentz, M. Fernández Ruiz, S. Foster, A. Muttoni, Background to the *fib* model code 2010 shear provisions – par i: beams and slabs, Structural Concrete 14 (2013) 195–203.

[66] A. Carpinteri, M. Corrado, Dimensional analysis approach to the plastic rotation capacity of over-reinforced conrete beams, Engineering Fracture Mechanics 77 (2010) 1091–1100.

[67] F. Cavagnis, M. Fernández Ruiz, A. Muttoni, Shear failures in reinforced concrete members without transverse reinforcement: An analysis of the critical shear crack development on the basis of test results, Engineering Structures 103 (2015) 157–173.